Physical Chemistry Chemical Physics

Dynamic Article Links ►

Cite this: DOI: 10.1039/c0xx00000x

ARTICLE TYPE

www.rsc.org/xxxxxx

Insights into mechanical compression and the enhancement in performance by $Mg(OH)_2$ coating in flexible dye sensitized solar cells

T. A. Nirmal Peiris,[a] K. G. Upul Wijayantha[a] and Jorge García-Cañadas*[b]

Received (in XXX, XXX) Xth XXXXXXXXX 20XX, Accepted Xth XXXXXXXXX 20XX

DOI: 10.1039/b000000x

The engineering of flexible dye sensitized solar cells (DSCs) by mechanical compression is one of the methods that allow low temperature processing of these devices. However, suppressing the high temperature sintering process also significantly reduces the performance of the cells. In our previous work [J. Phys. Chem. C, 116 (2012) 1211], we have attempted to improve flexible DSC performance by coating the porous TiO_2 photoanode with an electrodeposited $Mg(OH)_2$ layer. In that work, we have obtained one of the largest photovoltage reported to date in flexible DSCs (847 mV). In order to gain more insights into the reasons for both poorer performance of compressed cells and the origin of the voltage enhancement achieved by the $Mg(OH)_2$ coating, here we present an in-depth study by means of electrochemical impedance spectroscopy, Mott-Schottky plots analysis and open-circuit voltage decays. The existence of a shunt resistance in the mechanically compressed cells is revealed, causing an additional drawback to the poor inter-particle necking. By introducing the $Mg(OH)_2$ coating the recombination in the cell becomes significantly reduced, being the key reason which is responsible for the higher photovoltage. Additionally, the coating and the compression cause modifications in the surface states and in the nature of the interfaces with the electrolyte. This induces TiO_2 conduction band displacements and shifts of the relative position of the modified states that influence the performance.

Introduction

Exploration of lightweight and flexible renewable energy conversion devices is highly important in modern world because of their advantages as a low cost alternative to conventional silicon solar cells[1, 2] and their integration in advanced mobile applications and power devices.[3] Dye sensitized solar cells (DSCs) are considered a promising low cost technology and also have the potential to compete in the search for environmentally clean sources of electrical energy.[4]

In DSCs a nanostructured TiO_2 electrode is typically sintered at 450 ^oC on a glass substrate to obtain an interconnective semiconductor network that collects and transports the photo-injected electrons to the contact. It also provides a large area skeleton that allows abundant dye upload on the surface amplifying the photogenerated charge. Engineering the DSCs by mechanical compression is one of the available methods that allow low temperature processing of the cells.[5] This permits the use of plastic substrates[6] and roll to roll manufacturing at the same time that the energetic costs are reduced by the suppression of the high temperature sintering.[7, 8]

However, compared to glass based DSCs, low temperature processed flexible cells are far away behind in performance. One of the reasons for this behavior is the poor inter-particle and particle-substrate connection,[9] that leads to a poorer transport of injected electrons and increases the recombination rate, which occurs either from the substrate (back contact) or from the TiO_2.

Recently, many efforts have been made to improve the flexible DSC performance by using blocking layers prepared by low temperature deposition methods. Metal oxides (MgO, ZnO, Nb_2O_5, Al_2O_3, SiO_2, and ZrO_2),[10, 11] metal hydroxides ($Mg(OH)_2$, $Zn(OH)_2$, $Al(OH)_3$, and $La(OH)_3$)[12] and high band gap semiconductors[13] are widely employed to retard the recombination path ways from both the TiO_2 and the substrate. The promising results of our previously reported work confirmed that electrodeposition of a conformal $Mg(OH)_2$ insulating coating on the TiO_2 electrode improves the performance of flexible DSC.[14] Specially, a significant enhancement in photovoltage was achieved (847 mV). This is the highest voltage value reported to date for a treated flexible DSC.

In order to understand the origin of the higher performance provided by the $Mg(OH)_2$ coating and gain more insights into the reasons behind the lower performance of mechanically compressed cells, we present here a detailed analysis by means of electrochemical impedance spectroscopy (IS). Although IS is a well-known and widely used technique in the analysis of DSCs,[15] very few in-depth studies have been reported in flexible DSCs.[9] Most of the literature shows experimental results performed at open-circuit voltage (V_{oc}) or few dc voltage values,[16-18] which does not providing information on the events occurring in the rest

of the voltage region.

Our study analyses the impedance spectra at all the dc voltages in which the device operates, providing a more complete an accurate picture of the cells. For this purpose we discuss the electrical and operational differences in cells made with TiO_2 electrodes with and without $Mg(OH)_2$ coating and compression. We observe new features appearing due to the compression. Furthermore, we determine the origin of the photovoltage enhancement and identify the alteration of bandgap states in the coated cells. Electrical events (band displacements and energy shifts in bangap states) associated with the modification of the substrate/electrolyte interface are also discussed. Open-circuit voltage decays (OCVD) and Mott-Schottky plots are used to support the IS results as well. The new features analyzed provides a more clear understanding of the most relevant processes that cause the lower performance of flexible DSC which is key to identify new routes for improvement.

Experimental

Nanoporous TiO_2 thin film electrodes were prepared from a binder-free colloidal suspension of TiO_2 nanoparticles (P25, Degussa). Five consecutive layers of colloidal suspensions were dispersed on ITO-PEN substrates (13 Ω/□, Peccell Technologies, Inc., Japan) by doctor blade and compression methods.[19] The first TiO_2 layer was compressed at 80 MPa, the 3 following layers at 30 MPa, and the last layer was not compressed. An additional electrode formed by 5 non-compressed layers was also prepared for comparisons. TiO_2-coated ITO-PEN substrates were then heated at 140 °C for a 30 min period on the surface of a hotplate.[9]

A $Mg(OH)_2$ coating was electrodeposited on a TiO_2 electrode in an aqueous electrolyte solution composed of $Mg(NO_3)_2.6H_2O$ (Sigma Aldrich) having a concentration of 0.01 M.[9] The electrodeposition was carried out in a three electrode configuration using the TiO_2 coated ITO-PEN substrate as working electrode with 0.16 cm^2 area, Ag/AgCl electrode and Pt as the reference and counter electrodes, respectively. The working and counter electrodes were placed parallel to each other separated by a distance of approximately 1 cm in the electrodeposition solution. The electrodeposition was conducted at a constant current of -0.6 mA (chronopotentiometry) for 2 min using a Potentiostat-Galvanostat (Eco Chemie micro-Autolab type III). After the deposition, the films were removed from the electrolyte solution, washed with distilled water and allowed to dry at room temperature.

Non-deposited and $Mg(OH)_2$ deposited TiO_2 films were soaked overnight in an ethanolic solution of 1×10^{-6} M N719 (di-tetrabutylammoniumcis-bis(isothiocyanato)bis (2,2'-bipyridyl-4,4'-dicarboxylate) dye (Solaronix SA). The sensitized electrodes were sandwiched with a Pt/Ti alloy-PEN flexible counter electrode (5 Ω/□, Peccell Technologies, Inc., Japan) using a 25 µm thick Surlyn frame (Solaronix SA). The sandwiched cell was filled with the electrolyte through a hole in the counter electrode and sealed. The iodide/tri-iodide electrolyte comprising 0.4 M LiI, 0.4 M tetrabutylammonium iodide (TBAI), and 0.04 M I_2 dissolved in 0.3 M *N*-methylbenzimidazole (NMB) in acetonitrile (AN) and 3-methoxypropionitrile (MPN) solvent mixture at volume ratio of 1:1 was used. For the analysis, three different flexible DSCs were made using modified TiO_2 electrodes, that is, with (coated cell, CC), without $Mg(OH)_2$ coating (non-coated cell, NC) and a non-compressed (0MPa cell) as deposited electrode.

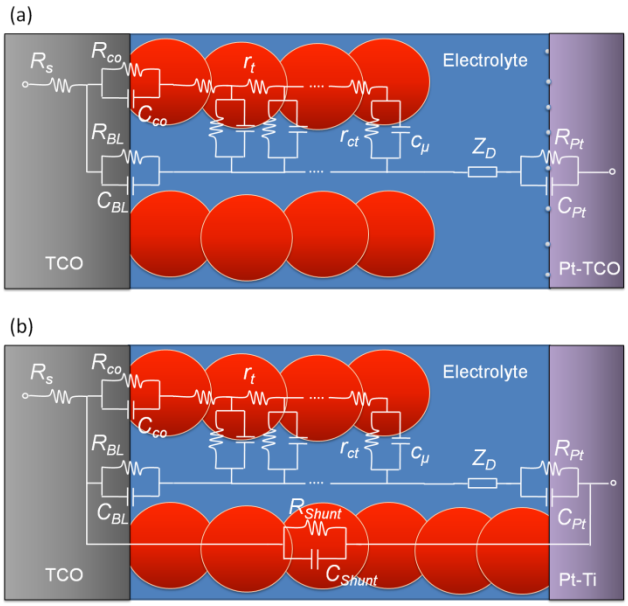

Fig. 1 Equivalent circuit that describes most of the processes that take place in a DSC (a). Equivalent circuit used for the analysis of the impedance results including an alternative shunt path (b).

Electrochemical experiments were carried out using a potentiostat (Eco Chemie Autolab PGSTAT302N). Steady-state current density–voltage (*j-V*) measurements of the cells were taken while the cells were illuminated at 100 $mWcm^{-2}$ light intensity. IS measurements were performed between 0 and -0.9 V at 0.05 V steps in the frequency range from 0.01 Hz to 1 MHz, both in the dark and under illumination. Results were analyzed using Zview Software. All the constant phase elements used in the fittings were converted to capacitance values using a reported procedure.[20] Illumination was achieved by means of a warm white LED light source (Floodlight, 50 Watt). The corresponding (*j-V*) plots were recorded using the same LED light source and also an AM 1.5 Class A solar simulator (Solar Light 16S – 300).

OCVD measurements were conducted by illuminating the cells with the solar simulator at 100 $mWcm^{-2}$ intensity until the photovoltage was stabilized. Then the light was turned off, and the open-circuit voltage was recorded at 50 ms intervals. All light intensities in all experiments were measured using a pyranometer (Solar Light Co., PMA2144 Class II).

Results and discussion

Most of the internal processes occurring in DSCs are described in IS by the electrical equivalent circuit of Fig. 1a.[21] The series resistance R_s accounts for the electrical resistance of the transparent conductive oxide (TCO), the electrical contacts and the wires. R_{co} and C_{co} are the resistance and capacitance at the contact between the TCO and the TiO_2 respectively. R_{BL} and C_{BL} describe the recombination processes in the TCO/electrolyte interface. The Z_D Warburg element relates to the diffusion of the redox species. The reduction process at the platinized counter electrode/electrolyte interface is described by the charge transfer

resistance (R_{Pt}) and the capacitance (C_{Pt}) at the interface. The processes that involve the TiO_2 film are described by the transmission line element. The microscopic transport resistance r_t accounts for the transport of electrons in the nanoparticles. The recombination process at the TiO_2/electrolyte interface is determined by the charge transfer resistance r_{ct} and the chemical capacitance c_μ (accumulation of charge in the density of states of the TiO_2).

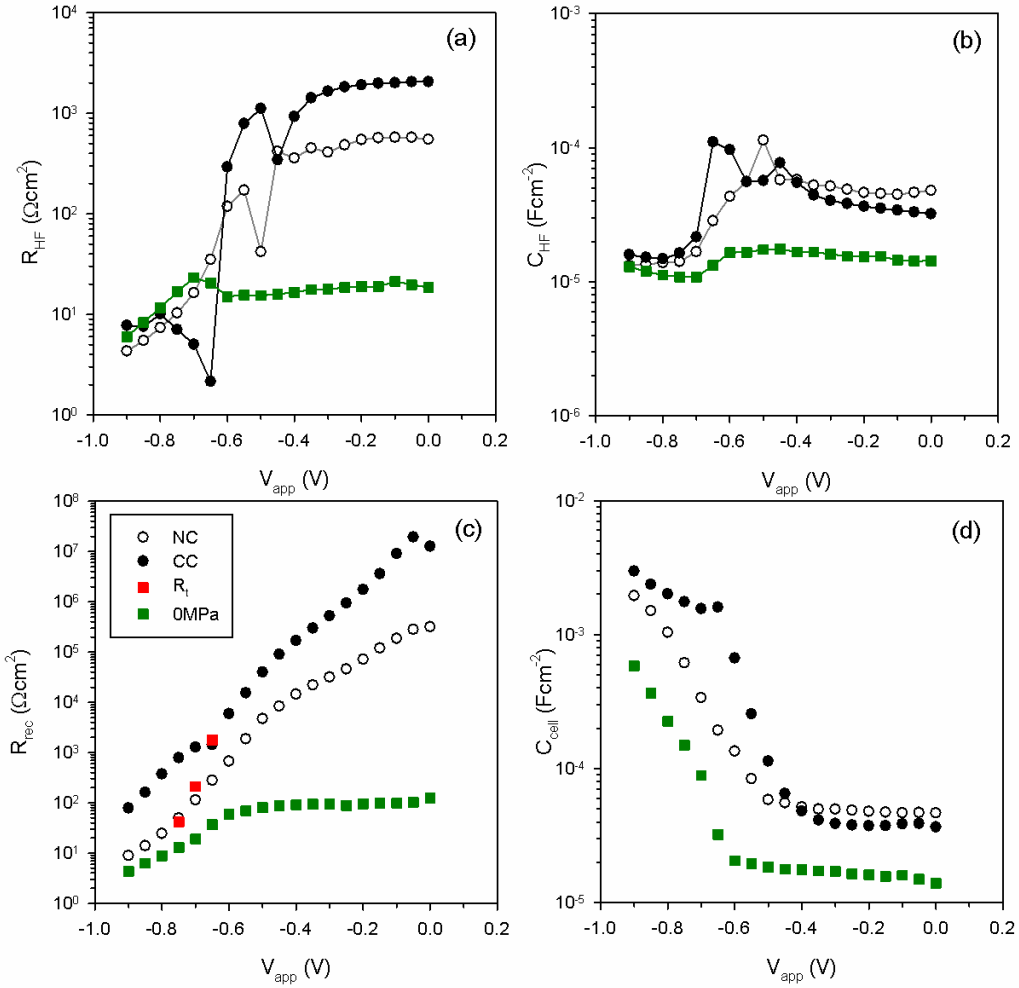

Fig. 2 Dark impedance results of non-compressed 0MPa cell (green squares), coated cell (CC, black circles) and non-coated cell (NC, white circles). The high frequency resistance R_{HF} (a), high frequency capacitance C_{HF} (b), recombination resistance R_{rec} (c), and cell capacitance C_{cell} (d) are plotted versus the applied potential V_{app}. In (c) the transport resistance R_t (red squares) from the coated cell (CC) is included

Our previous impedance analysis in the dark on flexible DSCs revealed that compression of TiO_2 electrodes causes significant differences in the high frequency region (left part) of the impedance spectra.[9] This region usually only indicates the oxidation of the redox mediator at the platinized counter electrode. This oxidation process is described by a semicircle consisting on the parallel combination of R_{Pt} and C_{Pt}. Since additional contributions to R_{Pt} and C_{Pt} values other than the oxidation process are expected, the high frequency semicircle is going to be determined by R_{HF} and C_{HF} in the present study. The processes that account for R_{HF} and C_{HF} vary from one cell to another, existing contributions from different origins as we will discuss accordingly below for each cell.

Fig. 2 shows the dark impedance results at the different applied voltages (V_{app}) for the three different cells prepared (0MPa, NC and CC) obtained by fitting to the equivalent circuit in Fig. 1b. The R_{rec} and C_{cell} elements account for the contribution at the interfaces where recombination takes place (r_{ct}/R_{BL} and c_μ/C_{BL} respectively) and R_{HF} and C_{HF} account for the combination of the shunt path, the counter electrode reaction and the ITO/TiO_2 contact ($R_{shunt}/R_{Pt}/R_{co}$ and $C_{shunt}/C_{Pt}/C_{co}$ respectively). The Warburg element (Z_D) values are not shown in Fig. 2 since they only appear at the most negative voltages and have a minor influence in the analysis. As we will remark later, the transport resistance R_t in the transmission line element was only used for the fitting in some of the spectra in the CC. In the rest of the analysis it did not show up.

Effects of mechanical compression

In order to gather information about the effects of the mechanical compression, we discuss in this section the differences between the non-compressed (0MPa) and the

compressed cell (CC). In the 0MPa cell the usual trend of R_{Pt} and C_{Pt} (nearly constant behavior) at voltages more positive than -0.6 V is observed (Figs. 2a and 2b), and this is the process responsible for the high frequency region response in the non-compressed cell (the shunt path does not appear). However, a deviation (small increase in R_{HF} and a slight decrease in C_{HF}) from this behavior appears when the applied voltage changes towards values more negative than -0.6V. This is due to the rise of the parallel combination of the contact resistance (R_{co}) and the contact capacitance (C_{co}) at the non-compressed ITO/TiO_2 contact, which agrees with the increase of C_{cell} due to c_μ (Fig. 2d) taking place at the same potential (i. e. electrons start to accumulate in the TiO_2 and to cross the TCO/TiO_2 interface). The parallel combination $R_{co}||C_{co}$ connecting in series with $R_{Pt}||C_{Pt}$, is responsible for the increase in R_{HF} and the decrease of C_{HF}.

The obtained C_{cell} in Fig. 2d exhibits the Mott-Schottky behavior of the cell at the more positive voltages and the exponential increment at more negative values than -0.6 V. However, there are two remarkable differences here with respect to standard liquid cells. (i) The onset voltage -0.6 V for the rise of C_μ is shifted around -0.2 V compared to the standard liquid cells where the onset usually occurs around -0.4 V.[21, 22] (ii) Additionally, R_{rec} (Fig. 2c) shows a small and nearly constant value in the Mott-Schottky region (V_{app}> -0.6 V) associated with strong recombination occurring at the ITO/electrolyte interface. A more steep exponential decrease of several orders of magnitude, as appearing at V_{app}< -0.6 V is typically observed in standard cells along the whole applied voltage range. Both (i) and (ii) are consequences of the non-compressed TiO_2 electrode which is primarily derived from poor nanoparticle segregation along the substrate and reduced particle-particle and particle-substrate connections. Since most of the nanoparticles remain aggregated in the film, the substrate area exposed to the electrolyte is higher, causing the strong recombination in the back layer and the upwards TiO_2 conduction band shift. (i.e. the -0.2 V shift of the c_μ onset). This is also observed in the Mott-Schottky analysis as we will discuss later.

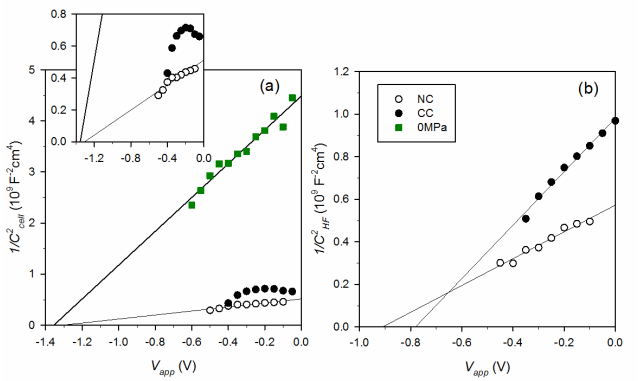

Fig. 3 – Mott-Schottky plots of C_{cell} (a) and C_{HF} (b) for the 0MPa (green squares), NC (white circles) and CC (black circles) cells. Inset plot in (a) shows a magnification for more clarification. Lines are linear regressions for each plot, except for the CC cell that shows no linear trend

The mechanical compression benefits to segregate the TiO_2 nanoparticles, to improve the ITO/TiO_2 contact, and the connection (necking) between the nanoparticles.[9] This process produces significant changes in the impedance spectra of the compressed NC cell as shown in Fig. 2. In the low frequency region (Fig. 2c and 2d), the onset of C_μ is now at -0.5 V, 100 mV more positive than the 0MPa cell, thus closer to standard DSCs. On the other hand, the value of the C_{cell} in the Mott-Schottky region (more positive voltages than -0.5 V) is significantly larger in the NC cell than in the 0MPa cell. Both facts are due to the reduction of the substrate area exposed to the electrolyte that modifies the potential drop in the Helmholtz layer. A Mott-Schottky plot of all cells is shown in Fig. 3. A significant reduction in the slope of the plots is observed when comparing the 0MPa and NC cells in Fig. 3a. This is due to a reduction in the area of the substrate/electrolyte interface caused by the segregation of the nanoparticles by the mechanical compression.[23] Regarding the exponential increase in the C_{cell} due to the c_μ, the slope is mainly determined by the density of states (DOS) in the bandgap (trap distribution).[24] As observed in Fig. 2d, both 0MPa and NC cells show similar slopes (parallel increase), pointing out that the DOS is not affected by the compression.

By looking at the R_{rec} values obtained for the NC cell, they are higher than in the 0MPa cell at all the applied voltages and show the usual exponential trend as in standard DSCs[24] (Fig. 2c). On the other hand, it is remarkable that sudden changes in R_{HF} (Fig. 2a) and C_{HF} (Fig. 2b) appear now in the high frequency region of the NC cell. A constant trend at the more positive voltages is followed by a sharp minimum at -0.5 V and then a decrease reaching the trend of the Pt counter electrode response at voltages more negative than -0.7 V is observed. We attribute this feature to a shunt resistance R_{shunt} (Fig. 1b), i. e. it exists in the cell an alternative path for the electrons to cross other than the usual route through recombination in Fig. 1a. This is produced by the direct contact of the TiO_2 with the counter electrode. This resistance depends mainly on the transport resistance in the TiO_2. For this reason it shows a constant trend until the film starts to accumulate electrons (V_{app} > -0.5 V). Then, the conductivity increases and hence also R_{shunt} in the typical exponential way of the TiO_2 transport resistance.[15] Once it reaches small values, the Pt resistance dominates at V_{app} < -0.7 V and a behavior similar to the 0MPa cell is observed. The sharp minimum at -0.5 V that relates to the maximum at the same voltage in C_{HF} (Fig. 2b) is due to a mono-energetic deep surface state[25] that frequently appears close to the voltage value of the onset of C_μ. Similar features appear in the R_{HF} reported in our previous study evaluating the influence on the mechanical compression where we suggested that a corrosion or degradation process could be responsible for the behavior observed.[9] However, the further analysis performed here points out to the existence of a shunt resistance as explained above.

The C_{HF} of the NC cell in Fig. 2b shows a Mott-Schottky trend at the more positive voltages as plotted in Fig. 3b. The apparent flatband potential is now far from the ≈-1.3 V value of ITO observed for C_{cell} (Fig. 3a). In contrast, it shows a value ≈-0.9 V, which is close to the flatband potential value of TiO_2.[26] This indicates that the C_{shunt} relates to the TiO_2/electrolyte interface when the film is in the dielectric state. When the accumulation of electrons takes place, C_{shunt} decreases since the chemical capacitance takes over at low frequencies (Fig. 2d) and the C_{Pt} then dominates the high frequency response as occurred with R_{HF}

(Fig. 2a).

The origin of the shunt resistance is not completely understood and further studies are needed to fully explain the phenomenon. We believe that the origin of the shunt resistance is due to movements in the TiO_2 network derived from the poor sintering and the flexibility of the substrates and/or to the pressure applied to the sandwiched electrodes during the sealing process. It seems that the shunt resistance is a consequence of the use of flexible substrates and it is more unlikely to appear in glass-based DSCs. This, in addition to the losses induced by the low-temperature sintering, could be the main reasons for the poorer performance observed in flexible DSCs when compared with their glass counterparts.

Effects of $Mg(OH)_2$ coating

When $Mg(OH)_2$ is electrodeposited onto the TiO_2 electrode (CC), a hydroxide layer is grown from the substrate area non-covered by TiO_2 nanoparticles that spreads filling the voids of the nanoporous matrix. By employing a deposition time of 2 min, the $Mg(OH)_2$ is expected to cover the areas of substrate in contact with the electrolyte and extend some monolayers along the nanoparticulate network.[14] Fig. 2 shows the changes produced in the dark impedance parameters by the coating process.

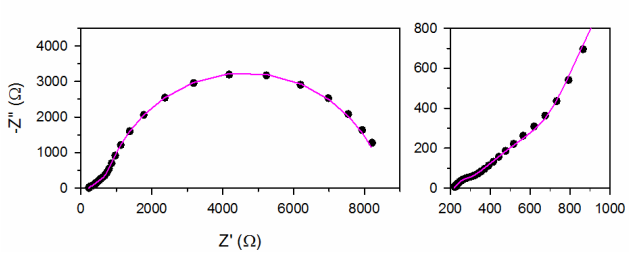

Fig. 4 Impedance spectrum in the dark of the cell coated with $Mg(OH)_2$ at -0.70 V (dots) and fitting to the spectrum (lines). The right plot shows a zoom at high frequency

By first looking at the C_{cell}, we observe that the onset of the C_μ is shifted ≈150 mV more positive when the cell is coated. This clearly states that the Helmholtz layer at the substrate/electrolyte interface has been modified by the electrodeposited $Mg(OH)_2$ coating. This is also observed in the Mott-Schottky plots in the inset of Fig. 3a, where the Mott-Schottky linear relation is lost due to the contribution of the coated layer to the total capacitance of the substrate/(electrolyte, TiO_2, $Mg(OH)_2$) interface.[23] At the more negative applied voltage region, the chemical capacitance of CC shows a peak at -0.65 V that it is not present in the NC (Fig. 2d). This peak produces a valley in the R_{rec}.[25] Similarly, a peak also appears in C_{HF} (Fig. 2b) at the same applied voltage value that relates to the minimum appearing in R_{HF} in the same voltage region (Fig. 2a). These features are due to the modification of TiO_2 surface states that become covered by the coating that has penetrated into the porous network, giving rise to a modified distribution.

The modified distribution of states also causes a distinctive feature at $-0.75 \leq V_{app} \leq -0.65$ V in the impedance spectra obtained for the CC due to the presence of R_t (red squares in Fig. 2c) which was not visible in the rest of the cells. Fig 4 shows the spectrum of the cell with the clear linear trend due to this transport resistance observed at mid frequencies, which vanishes at -0.8 V. R_t appears due to the quicker accumulation of electrons occurring in part of the modified surface states, since a peak appears now in the C_{HF} instead of the decrease shown by the NC cell (Fig. 2b). The fact that the transport through the shunt is now influenced by this charge accumulation produces the linear trend in the spectra and the sharp peak in R_{HF}, which drops to very small values that correspond to the contact resistance R_{co} since the R_{shunt} is now described by R_t at mid frequencies.

At $V_{app} < -0.8$ V, the influence of the coated states is no longer significant and the high frequency parameters show the same trend as the Pt counter electrode response (Figs. 2a and 2b). We remark that R_t is usually observed at voltages close to the onset of C_μ which it is when the electron concentration starts to increase in the conduction band.[27] However, in the CC it appears at voltages far from the onset region (-0.65 V). This is due to the influence of the modified surface states that are located in the part of the film close to the substrate, where the coating extends.

Another relevant change produced by the effect of the $Mg(OH)_2$ coating is the significant increase of the shunt resistance (Fig. 2a) and decrease of the recombination along the whole voltage range (R_{rec} increase in Fig. 2c). This largely benefits the cell performance and proves the successful operation of the introduced coated layer. As occurred in the NC cell, the presence of deep surface sates which produce the small peaks in R_{HF} and C_{HF} (Figs. 2a and 2b) also appears. Nevertheless, it is slightly shifted 50 mV positively in the CC respect to NC due to the modification of the Helmholtz double layer produced by the coating.

The comparison carried out from dark impedance results have revealed a significant number of features produced by the coating layer. However, in order to evaluate how the cells behave under actual operating conditions, experiments under illumination are required.

Analysis of device performance under illumination

Fig. 5a shows the *j-V* characteristics of the NC and CC cells. As can be seen in the inset of the figure a decrease in the photocurrent (j_{sc}) and an increase in the photovoltage (V_{oc}), fill factor (*FF*) and efficiency (η) were produced by the $Mg(OH)_2$ coating. Note that the performance of the cells observed in Fig. 5a are lower than in our previous work[14] due to the use of a LED light source. When solar simulated light is used similar results to those reported were obtained (Fig. 5b).

The decrease in the photocurrent observed in the CC can be explained by a reduction of the amount of adsorbed dye, occurring since the $Mg(OH)_2$ penetrates some extent along the voids of the nanoparticulate network. This was proved by internal surface area and IPCE experiments in our previous article.[14]

Fig. 6 shows the impedance results under illumination for the NC and CC cells. A general decrease of all the resistance values with respect to the dark results (Fig. 2) is observed. The R_{HF} decreases around one order of magnitude and the R_{rec} even higher, especially at the more positive voltages (Figs. 6a and 6c). This is due to the fact that the photo-injected electrons make the Fermi level no longer homogeneous along the film as in the dark measurements. Therefore, the electron concentration and conductivity of the TiO_2 is higher and non negligible even at the more positive voltages. This also makes more difficult to distinguish the processes that appeared in the dark results. In the

high frequency part both CC and NC cells reach the Pt counter electrode behavior at voltages more negative than -0.6 V (Figs. 6a and 6b), and the effect of the modified surface state distribution induced by the coating is shifted to the more positive voltage region (V_{app} > -0.4 V) and additionally broadens, causing the larger C_{HF} values and the maximum in R_{HF}. The small peaks due to deep surface states in both cells in C_{HF} appear at -0.25 V and -0.45 V for the NC and CC cells respectively, producing the small minimums in R_{HF} at the same voltage values. As observed in the dark measurements (Fig. 2a), the $Mg(OH)_2$ coating increases R_{shunt} in the CC cell, especially in the -0.4 V < V_{app} < -0.1 V region (Fig. 6a). This leads to the higher field factor observed in the CC.

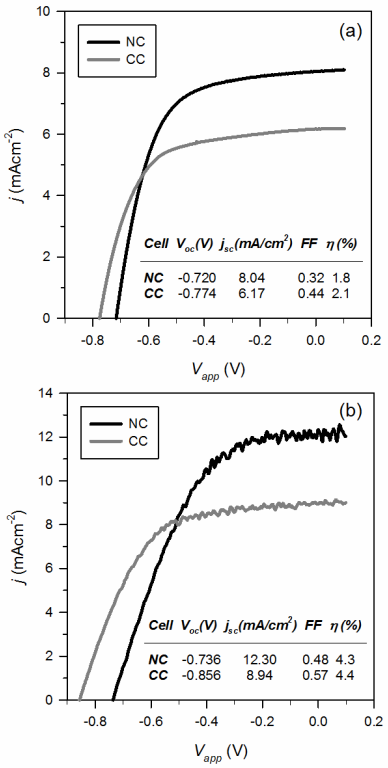

Fig. 5 *j-V* curves of mechanically compressed cells with $Mg(OH)_2$ layer (CC, grey) and without (NC, black) under 100 mW/cm^2 LED illumination (a) and solar simulated light (b) from a Solar Light 16S-300, AM1.5G, Class A simulator

The recombination resistance is higher for the whole potential range (except a small region at the more positive voltages) for the CC cell due to the coating as occurred in the dark measurements. This improvement points out to be responsible for the enhancement achieved in the photovoltage by the $Mg(OH)_2$ coating layer. However, the displacement of the conduction band position in the TiO_2 has to be also taken into account. For this purpose, in Fig. 7 R_{rec} and C_{cell} are plotted versus the Fermi level voltage V_F, which represents the voltage drop in the cell due to the separation of the quasi-Fermi levels of electrons (E_{Fn}) and holes (E_{redox}), i. e. $V_F=(E_{Fn}-E_{redox})/q$, where q is the elementary charge.[24] V_F is obtained by subtracting the voltage drop in the total series resistance R_{TS} from the applied voltage, $V_F=V_{app}-jR_{ST}$. The total series resistance is given by $R_{ST}=Rs+R_{HF}+R_D$, being R_D the diffusion resistance extracted from Z_D. Fig. 7b reveals that the coating layer shifts the conduction band position. In order to quantify this shift (ΔE_c) and properly compare both NC and CC cells, R_{rec} and C_{cell} are plotted versus an "equivalent conduction band" potential V_{ecb} in Figs. 7c and 7d.[24] ΔE_c is obtained by displacing -30 mV the V_F for C_{cell} in the CC in order to become superpose to NC. The V_{ecb} is calculated as $V_{ecb}=V_F-\Delta E_c$. Fig. 7c reveals the actual recombination kinetics, which is higher than what was initially observed in Fig. 6c. From this analysis it can be concluded that despite of the presence of a downwards displacement of the conduction band of 30 mV, the recombination kinetics is much slower in the CC. This leads to the significant V_{oc} enhancement observed in this cell.

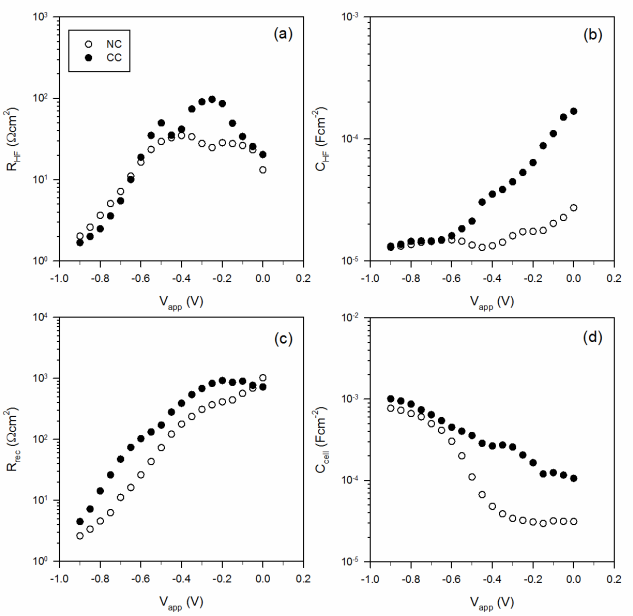

Fig. 6 Impedance results under illumination for the non-coated (NC, white) and coated (CC, black) cells. R_{HF} (a), C_{HF} (b), R_{rec} and C_{cell} (d) are plotted versus the applied potential

Fig. 8 shows the electron lifetime obtained from OCVD experiments performed in both NC and CC cells. A significant increase is observed due to the coating, in agreement with the impedance results. Moreover, the lifetime curve in the CC shows the linear trend at the more negative voltages indicating the influence of recombination from the conduction band, what it is not observed for the NC cell that shows the parabolic trend due to the main recombination taking place through the surface states.[26] This indicates that the E_{Fn} raises much higher (closer to the conduction band) in the CC cell, hence providing a higher V_{oc} despite of the 30 mV downwards shift of the conduction band.

Conclusions

An in-depth study based on IS results in mechanically compressed flexible DSCs have been performed. The comparisons carried out between a non-compressed cell (0MPa) and a non-coated compressed cell (NC) revealed new features appearing in the high frequency response induced by the compression, such as the presence of a shunt resistance. This could be a reason for the poorer performance of flexible DSCs respect to standard glass DSCs. Additionally, contributions due to the ITO/TiO_2 contact where also evaluated.

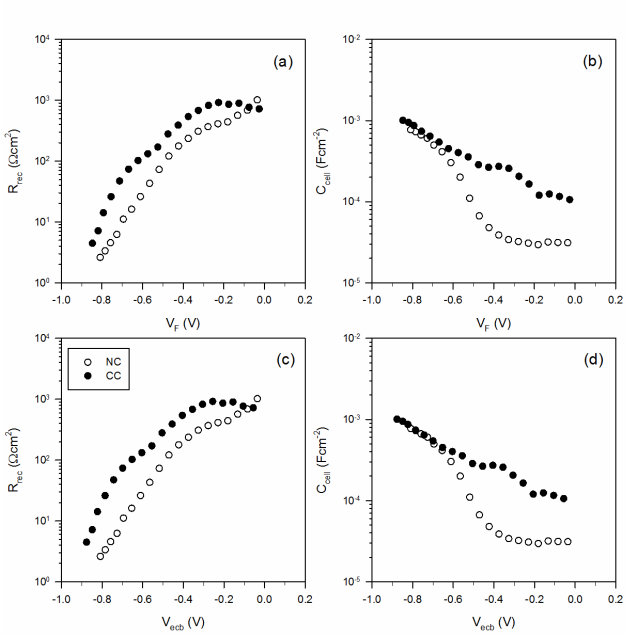

Fig.7 Representation of the light impedance results from Fig. 6 versus the Fermi Level voltage V_F (a, b) and the equivalent conduction band potential V_{ecb} (c, d)

When an electrochemically deposited $Mg(OH)_2$ coating is applied on the photoanode, a modification of surface states in the TiO_2 occurs and the shunt and recombination resistances increase due to the blocking effect. The coated cell exhibited a reduction of photocurrent in addition to a large gain in photovoltage. The lower dye uptake caused by the TiO_2 nanoparticles being coated is the main reason behind the photocurrent decrease. A downwards shift of 30 mV in the conduction band position of TiO_2 in the coated cell occurs. However, the higher recombination rate is more significant and prevails, leading to the V_{oc} enhancement. OCVD are in agreement with these results and also show much higher electron lifetimes for the CC.

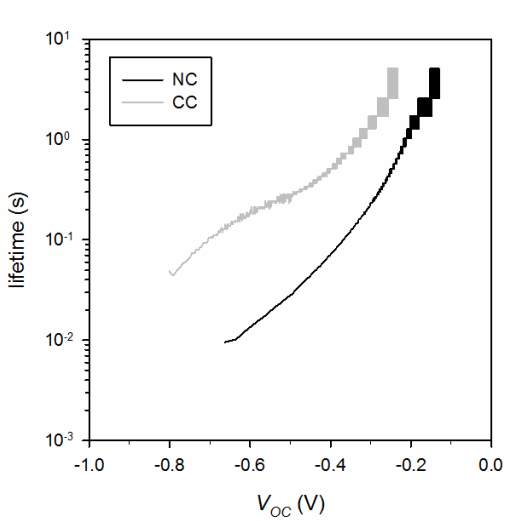

Fig. 8 Electron recombination lifetime obtained from OCVD measurements for the non-coated (NC, black) and coated (CC, grey) cells

Acknowledgements

This work was supported by UK EPSRC, DSTL, Johnson Matthey Plc and Department of Chemistry, Loughborough University. All members of renewable energy research group in the Department of Chemistry, Loughborough University are acknowledged for their assistance for this work. The authors would like to acknowledge previous related work conducted by S. Senthilarasu.

Notes and references

[a] *Department of Chemistry, Loughborough University, Loughborough, LE11 3TU, UK.*
[b] *Cardiff School of Engineering, Cardiff University, The Parade, Cardiff, CF24 3AA, UK. Tel:+44 (0)2920 8759 18; E-mail: garciacanadasj@cardiff.ac.uk*

1. B. Oregan and M. Gratzel, *Nature*, 1991, **353**, 737-740.
2. L. Y. Han, A. Islam, H. Chen, C. Malapaka, B. Chiranjeevi, S. F. Zhang, X. D. Yang and M. Yanagida, *Energy & Environmental Science*, 2012, **5**, 6057-6060.
3. A. Nathan, A. Ahnood, M. T. Cole, S. Lee, Y. Suzuki, P. Hiralal, F. Bonaccorso, T. Hasan, L. Garcia-Gancedo, A. Dyadyusha, S. Haque, P. Andrew, S. Hofmann, J. Moultrie, D. P. Chu, A. J. Flewitt, A. C. Ferrari, M. J. Kelly, J. Robertson, G. A. J. Amaratunga and W. I. Milne, *Proceedings of the Ieee*, 2012, **100**, 1486-1517.
4. J. Q. Peng, L. Lu and H. X. Yang, *Renewable & Sustainable Energy Reviews*, 2013, **19**, 255-274.
5. H. C. Weerasinghe, F. Z. Huang and Y. B. Cheng, *Nano Energy*, 2013, **2**, 174-189.
6. D. J. Lipomi and Z. A. Bao, *Energy & Environmental Science*, 2011, **4**, 3314-3328.
7. G. Hashmi, K. Miettunen, T. Peltola, J. Halme, I. Asghar, K. Aitola, M. Toivola and P. Lund, *Renewable & Sustainable Energy Reviews*, 2011, **15**, 3717-3732.
8. J. C. Tinguely, R. Solarska, A. Braun and T. Graule, *Semiconductor Science and Technology*, 2011, **26**, 045007.
9. S. Senthilarasu, T. A. N. Peiris, J. Garcia-Canadas and K. G. U. Wijayantha, *Journal of Physical Chemistry C*, 2012, **116**, 19053-19061.
10. A. Kay and M. Gratzel, *Chemistry of Materials*, 2002, **14**, 2930-2935.
11. E. Palomares, J. N. Clifford, S. A. Haque, T. Lutz and J. R. Durrant, *Journal of the American Chemical Society*, 2003, **125**, 475-482.
12. J. H. Yum, S. Nakade, D. Y. Kim and S. Yanagida, *Journal of Physical Chemistry B*, 2006, **110**, 3215-3219.
13. X. Z. Liu, L. Wang, Z. S. Xue and B. Liu, *Rsc Advances*, 2012, **2**, 6393-6396.
14. T. A. N. Peiris, S. Senthilarasu and K. G. U. Wijayantha, *Journal of Physical Chemistry C*, 2012, **116**, 1211-1218.
15. J. Bisquert and F. Fabregat-Santiago, in *Dye-sensitized Solar Cells*, ed. K. Kalyanasundaram, CRC Press, 2010, ch. 12, p. 457.
16. C. Longo, A. F. Nogueira, M. A. De Paoli and H. Cachet, *Journal of Physical Chemistry B*, 2002, **106**, 5925-5930.
17. X. Li, H. Lin, J. B. Li, X. X. Li, B. Cui and L. Z. Zhang, *Journal of Physical Chemistry C*, 2008, **112**, 13744-13753.

18. K. Miettunen, J. Halme, P. Vahermaa, T. Saukkonen, M. Toivola and P. Lund, *J. Electrochem. Soc.*, 2009, **156**, B876-B883.
19. T. Yamaguchi, N. Tobe, D. Matsumoto, T. Nagai and H. Arakawa, *Sol. Energy Mater. Sol. Cells*, 2010, **94**, 812-816.
20. Y. Y. Proskuryakov, K. Durose, M. K. Al Turkestani, I. Mora-Sero, G. Garcia-Belmonte, F. Fabregat-Santiago, J. Bisquert, V. Barrioz, D. Lamb, S. J. C. Irvine and E. W. Jones, *Journal of Applied Physics*, 2009, **106**, 9.
21. Q. Wang, S. Ito, M. Gratzel, F. Fabregat-Santiago, I. Mora-Sero, J. Bisquert, T. Bessho and H. Imai, *Journal of Physical Chemistry B*, 2006, **110**, 25210-25221.
22. F. Fabregat-Santiago, J. Bisquert, E. Palomares, L. Otero, D. B. Kuang, S. M. Zakeeruddin and M. Gratzel, *Journal of Physical Chemistry C*, 2007, **111**, 6550-6560.
23. F. Fabregat-Santiago, G. Garcia-Belmonte, J. Bisquert, P. Bogdanoff and A. Zaban, *J. Electrochem. Soc.*, 2003, **150**, E293-E298.
24. F. Fabregat-Santiago, G. Garcia-Belmonte, I. Mora-Sero and J. Bisquert, *Phys. Chem. Chem. Phys.*, 2011, **13**, 9083-9118.
25. J. Bisquert, F. Fabregat-Santiago, I. Mora-Sero, G. Garcia-Belmonte, E. M. Barea and E. Palomares, *Inorganica Chimica Acta*, 2008, **361**, 684-698.
26. J. Bisquert, A. Zaban, M. Greenshtein and I. Mora-Sero, *Journal of the American Chemical Society*, 2004, **126**, 13550-13559.
27. F. Fabregat-Santiago, J. Bisquert, L. Cevey, P. Chen, M. K. Wang, S. M. Zakeeruddin and M. Gratzel, *Journal of the American Chemical Society*, 2009, **131**, 558-562.

